Plasma Physics and Controlled Fusion

PAPER • OPEN ACCESS

Influence of the magnetic configuration on the high-field side scrape-off layer at ASDEX Upgrade and the role of the secondary separatrix

To cite this article: D Hachmeister *et al* 2024 *Plasma Phys. Control. Fusion* **66** 055016

OPEN ACCESS
IOP Publishing
Plasma Physics and Controlled Fusion
Plasma Phys. Control. Fusion **66** (2024) 055016 (10pp)
https://doi.org/10.1088/1361-6587/ad3a9f

Influence of the magnetic configuration on the high-field side scrape-off layer at ASDEX Upgrade and the role of the secondary separatrix

D Hachmeister[1,*], C Silva[1], J Santos[1], G D Conway[2], L Gil[1], A Silva[1], U Stroth[2,3], J Vicente[1], E Wolfrum[2], R M McDermott[2], R Dux[2], D Brida[2], R Fischer[2], B Kurzan[2], the ASDEX Upgrade Team[4] and the EUROfusion MST1 Team[5]

[1] Instituto de Plasmas e Fusão Nuclear, Instituto Superior Técnico, Universidade de Lisboa, 1049-001 Lisboa, Portugal
[2] Max-Planck-Institut für Plasmaphysik, Boltzmannstr. 2, 85748 Garching, Germany
[3] Physik-Department E28, Technische Universität München, 85747 Garching, Germany

E-mail: daniel.hachmeister@tecnico.ulisboa.pt

Received 18 October 2023, revised 14 March 2024
Accepted for publication 4 April 2024
Published 12 April 2024

Abstract
In tokamaks, radial transport is ballooning, meaning it is enhanced at the low-field side (LFS). This work investigates the effect of the magnetic configuration on the high-field side (HFS) scrape-off layer. Our experiments involved L-mode and H-mode discharges at ASDEX Upgrade, in which we scanned the magnetic configuration from a lower to an upper single-null shape, thus varying the location of the secondary separatrix. We show that the secondary separatrix determines the width of the HFS scrape-off layer, meaning that the density is much lower in the region that is magnetically disconnected from the LFS scrape-off layer, outside the secondary separatrix. Furthermore, we observe that the large density often seen in the HFS divertor drastically decreases as the separation between the primary and secondary separatrices falls below a particular value. This value is different for L-mode and H-mode plasmas and closely matches the power decay length measured at the LFS midplane. We also show how the HFS scrape-off layer density is smaller in an upper single-null than in a lower single-null, when the ionic grad-B drift points down. This difference is likely caused by reversing the $E \times B$ drifts in the active divertor when switching the active X-point from the bottom to the top. We further observe that the neutral density in the lower divertor also correlates with the plasma shape and the high-density region in the HFS scrape-off layer. During the shape scans analyzed here, the HFS divertor remained partially detached throughout, with transitory reattachment modulated by ELM activity in H-mode. This work provides novel experimental data that can be leveraged to further the modeling capabilities and understanding of scrape-off layer physics in highly shaped plasmas.

[4] See author list of H. Zohm *et al* 2024 *Nucl. Fusion* https://doi.org/10.1088/1741-4326/ad249d.
[5] See Labit *et al* 2019 (https://doi.org/10.1088/1741-4326/ab2211) for the EUROfusion MST1 Team.
[*] Author to whom any correspondence should be addressed.

Keywords: SOL, high-field side, high-density region, ASDEX Upgrade, reflectometry, double-null

1. Introduction

Optimizing plasma confinement and overall performance in tokamaks requires a good understanding of radial transport and scrape-off layer (SOL) dynamics. Radial transport in tokamaks is ballooning, meaning that it is more prominent on the low-field side (LFS) where the magnetic curvature is unfavorable [1–3]. Consequently, most charged particles cross the plasma boundary and enter the SOL on the LFS. The dominant parallel transport in the SOL directs particles along the field lines to the high-field side (HFS) and LFS divertor targets in single-null configurations [4]. In contrast, the double-null configuration magnetically isolates the HFS SOL from the LFS SOL, leading to significant asymmetries between the two [1].

Despite diagnostic limitations at the HFS, observations in different devices have confirmed that the turbulence drive is ballooning-like either through direct measurement at the LFS and HFS [5] or by performing discharges limited at different poloidal locations [6, 7]. Experiments on the Alcator C-Mod tokamak have demonstrated that the fluctuation-induced cross-field transport in the HFS SOL is low compared to the LFS SOL, leading to steep density and temperature profiles at the HFS SOL midplane [5].

Radial transport, however, is not the only difference between the HFS and the LFS. ASDEX Upgrade usually exhibits a region of high density and low temperature at the HFS divertor, located in the volume between the X-point and the HFS divertor target. The HFS SOL density near the X-point is typically one order of magnitude larger than the LFS midplane separatrix density [8]. This is the so-called high-density front, or high-density region of the HFS.

The high-density region in the HFS divertor is sustained by the parallel heat conducted from the LFS midplane and by the drift-driven cross-field particle fluxes from the LFS divertor resulting from $E \times B$ drifts [9–11]. The high-density region depends on the available heat flux reaching the region of strong ionization at the HFS divertor and forms with sufficient heating power [8, 12]. Both the parallel heat and the cross-field transport lead to increased ionization sources in the HFS divertor volume and augment the HFS neutral fluxes above the X-point, as reproduced by SOLPS modeling [10]. These modeling efforts have confirmed the crucial role of drifts in replicating the high-density region, as they contribute to particle fluxes towards the HFS divertor, thereby increasing ionization sources in the HFS far-SOL [10]. Current models successfully reproduce both the magnitude and extension of the high-density region, from the HFS target to the HFS midplane, aligning with experimental observations [13].

It has been shown, both experimentally and in simulation, that the magnitude of the HFS high-density region decreases with nitrogen seeding [10, 12]. The increased radiation in the HFS SOL leads to a reduced power in the region of strong ionization, reducing the ionization source in the HFS SOL. The ionization in the HFS divertor is limited by the available energy for ionization and impurity radiation, resulting in the power starvation of the recycling process as discussed in [10, 14, 15]. Both experimental and simulation data suggest that the high-density region in the HFS divertor is a source of neutrals that sustain the high neutral pressures in the HFS divertor [10, 12].

Experiments at ASDEX Upgrade have additionally discovered that, although first observed in the HFS divertor, the high-density front also extends upwards to the HFS SOL midplane where it leads to abnormally high densities [13, 16]. The high-density front is responsible for HFS/LFS asymmetries in the midplane SOL density and may cause inverted density gradients just outside the separatrix at the HFS midplane, as observed in modeling [10] and experiment [17].

This study investigates the evolution of divertor detachment and the high-density front in highly shaped plasmas close to the double-null configuration, which is typical to many reactor concepts [18–20]. We performed L- and H-mode experiments where we gradually scanned the magnetic configuration from a lower single-null to an upper single-null shape, passing through a double-null, while monitoring the detachment state and the magnitude and location of the high-density front. The results presented in this paper show that the HFS SOL density profile experiences significant changes during the shape scan. The profile narrows, and the density decreases as the plasma approaches a double-null shape.

2. Methods

In the following section, we describe the diagnostic methodology and the experiments performed at ASDEX Upgrade.

2.1. Diagnostics

We used an O-mode microwave reflectometry system to measure the density profile at the HFS and LFS, covering a density range of $0.3 - 3.0 \times 10^{19}$ m^{-3} with a temporal resolution of 35 μs [21]. As the reflectometer cannot measure densities below 0.3×10^{19} m^{-3}, it requires an estimate for the unmeasured part of the density profile [22]. This estimate can come from other edge diagnostics such as the edge Thomson scattering system [23].

In addition to the reflectometer, we used the following diagnostics: (i) Langmuir probes measuring the spatially resolved electron temperature and density along the divertor target with

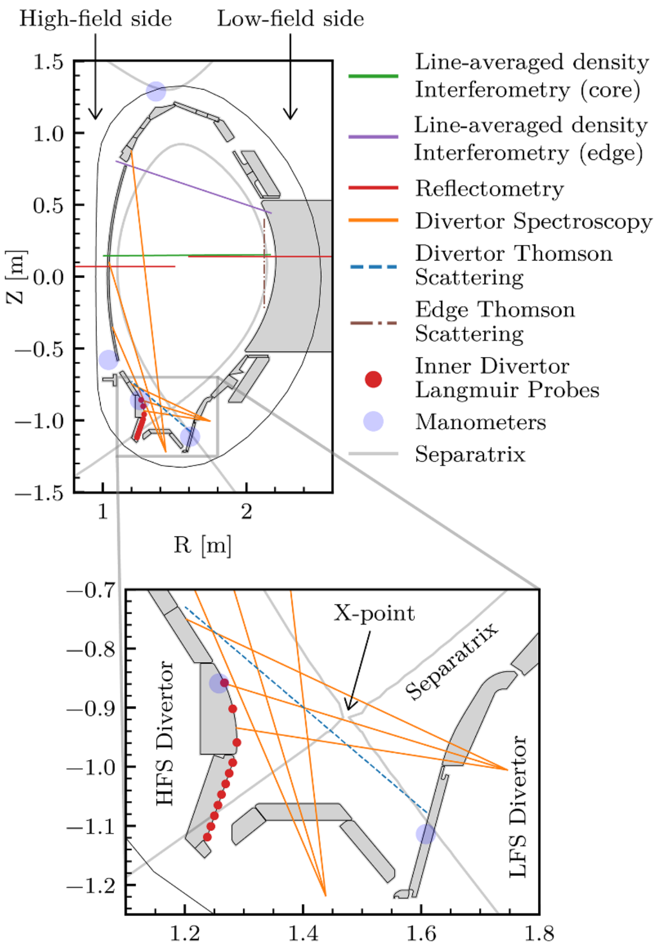

Figure 1. Cross-section of the ASDEX Upgrade tokamak showing the location and lines of sight of the diagnostics used in this work overlaid with the separatrix of a typical lower single-null plasma configuration.

a temporal resolution of 45 μs and a spatial resolution in the order of a couple of centimeters [24]; (ii) Stark broadening spectroscopy measuring the electron density in the divertor volume, determined by the spectroscopic measurement of the Stark broadened D_δ line, providing approximately the maximum electron density along each line of sight (LoS) with a temporal resolution that depends on the chosen integration time [8]—for our L-mode shots the resolution was 50 ms while for the H-mode shots it was 3 ms; (iii) Divertor Thomson scattering measuring the spatially resolved electron temperature and density along a fixed LoS crossing the divertor region with a laser repetition period of 50 ms and a spatial resolution of roughly one centimeter [25]; (iv) ionization gauges (manometers) to measure the neutral pressure in several vessel locations with a temporal resolution of 1.5 ms [26]. Figure 1 illustrates the location and LoS of the various diagnostics employed in this study.

2.2. Experiments

We performed experiments in both L- and H-mode at different deuterium fueling and nitrogen seeding levels to vary

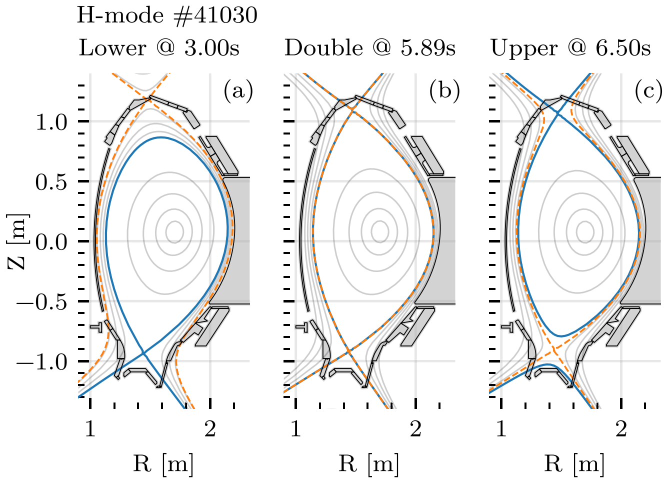

Figure 2. Magnetic equilibrium snapshots during a shape scan in H-mode (#41030). Primary separatrix (blue solid) and secondary separatrix (orange dashed). Lower single-null (a), double-null (b), and upper single-null (c).

the detachment state and overall plasma density. In all experiments we had the $B \times \nabla B$ direction point downwards. Regimes with high density or high input power are not explored in this study due to diagnostic limitations. These regimes would have a too large density in the HFS SOL, unmeasurable with the current reflectometry system, which is the only diagnostic available at the HFS midplane. For the same reason, the experiments were seeded with nitrogen since this reduces the density front magnitude, keeping the density within measuring range [12]. Having said this, all the experiments reported here have a high-density front or region.

Figure 2 shows three snapshots of a shape scan corresponding to the lower single-null, double-null, and upper single-null configurations. The figure also shows the two flux surfaces that pass through each X-point, i.e. the primary separatrix (blue) and the secondary separatrix (orange). The secondary separatrix, which is the last flux surface connecting the HFS and LFS SOL, strongly influences the HFS SOL density profile, as will be discussed later. The schematic illustration in figure 3 shows the various SOL and divertor regions and the terminology used in this article. Of particular importance is the region indicated as number 2, which is the SOL region where the HFS is 'connected' to the LFS. It will be shown in this article that region 2 on the HFS is where the high-density front exists. The high-density front is most intense at the height of the X-point, as schematically illustrated, expanding along the connected region (region 2) at least up to the HFS midplane where it is measured by profile reflectometry. Owing to the plasma shape's importance for this study, we relied on the so-called IDE equilibrium which uses a thermal and fast ion pressure constraint and a current diffusion equation [27].

Figures 4 and 5 show the time traces of two representative experiments, one in L-mode and one in H-mode. Both shots had a magnetic field of 2.5 T and a plasma current of 0.8 MA. The L-mode shot had 0.3 MW of ECRH and a q_{95} of 5.2 – 5.5.

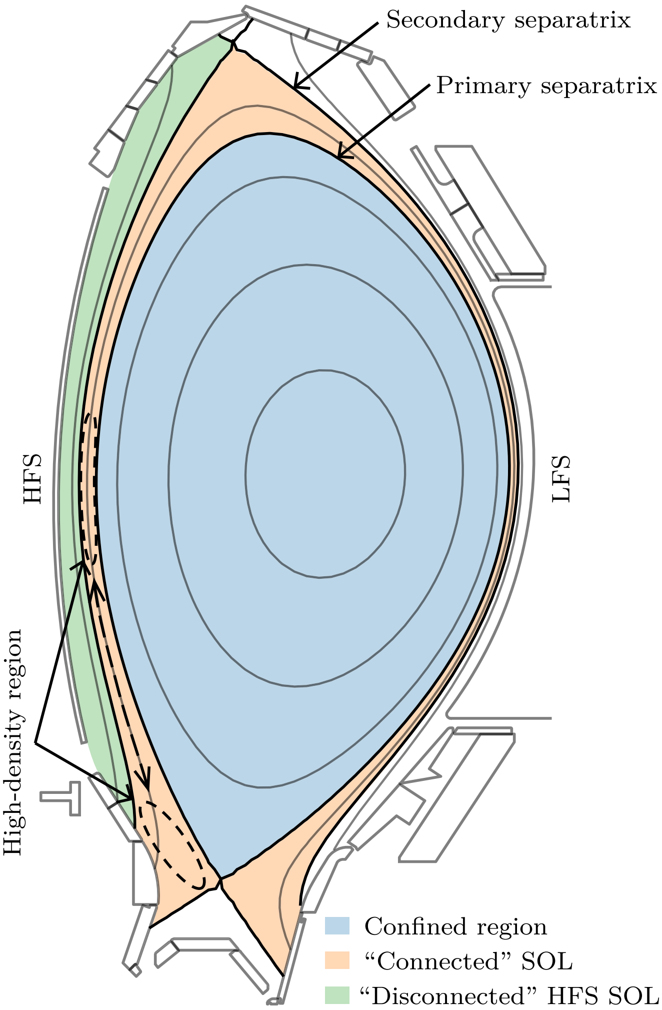

Figure 3. Schematic illustration of the different SOL and divertor regions: Confined region (blue); 'Connected' region of the SOL (orange); 'Disconnected' region of the HFS SOL (green). The 'connected' region lies between the primary and secondary separatrices (black solid lines). The high-density region (black dashed ellipses) at ASDEX Upgrade is measured at the HFS divertor using divertor diagnostics and at the midplane using profile reflectometry. The high-density front is most intense near the X-point and expands along the 'connected' region of the HFS SOL region at least up to the midplane where is has a lower intensity.

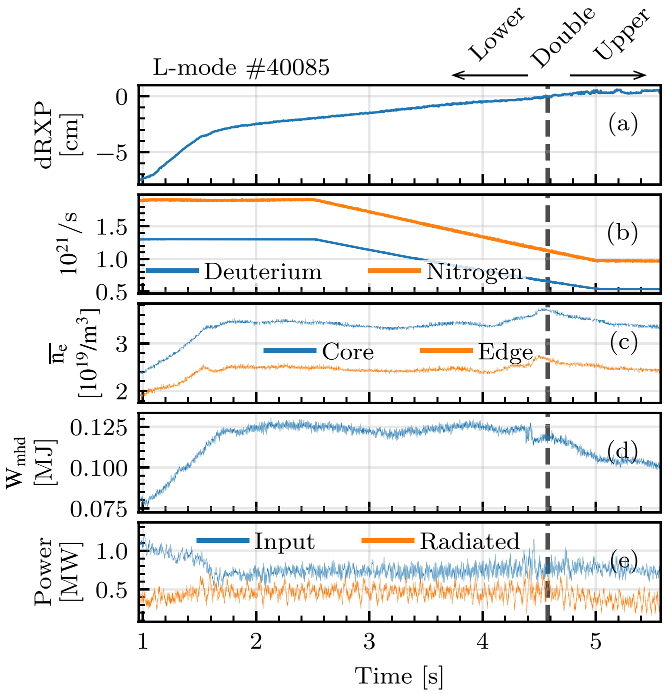

Figure 4. Main plasma parameters for the L-mode configuration scan #40085 with a magnetic field of -2.5 T, a plasma current of 0.8 MA, an ECRH heating power of 0.3 MW, and a q_{95} between 5.2 and 5.5. (a) separation between the first and second separatrix at the LFS midplane dRXP; (b) deuterium and nitrogen fueling rate; (c) core and edge line-averaged density; (d) stored energy; (e) total input and radiated power. The black vertical dashed line indicates the double-null phase.

The H-mode shot had 1.8 MW of ECRH and 2.5 MW of NBI heating and a q_{95} of $5.2-6.0$.

In figures 4 and 5, the parameter dRXP shown in panel (a) quantifies the plasma shape. The dRXP parameter is defined as the difference between the radial positions (dR) of the flux surfaces containing the lower and upper X-points (XP), respectively, measured at the LFS midplane. The dRXP parameter measures, therefore, the radial separation between the primary and secondary separatrix at the LFS midplane. As dRXP increases from negative to positive values, the plasma shape transitions from lower to upper single-null, with a double-null shape corresponding to a dRXP of zero.

During each experiment, we reduced the fueling rate shown in panel (b), which is necessary because vacuum pumps are only available in the lower divertor, resulting in poor pumping efficiency during the upper single-null phase. Particle recycling is higher in the upper divertor, and a smaller gas fueling rate is typically enough to maintain the core line-averaged density in upper single-null. Nevertheless, despite our efforts to maintain a constant line-averaged density, we often experienced an increase when approaching double-null, see panel (c). We used nitrogen seeding—see panel (b) - to mitigate the high-density region which was nevertheless present in our shots.

The stored energy, shown in panel (d), decreases in upper single-null, both in L- and H-mode, due to a reduction in confinement for this configuration. The total input power and total radiated power are shown in panel (e). The radiated power remained roughly constant during the lower single-null phase, decreasing slightly in upper single-null for both the L and H-mode shots.

In H-mode, the edge-localized modes (ELMs) evolve during the shape scan, as indicated in figure 5(f) by the divertor shunt currents measured at the HFS and LFS targets. The ELM amplitude decreases during the discharge with small and frequent ELMs near the double-null phase, with a frequency of about 250 Hz.

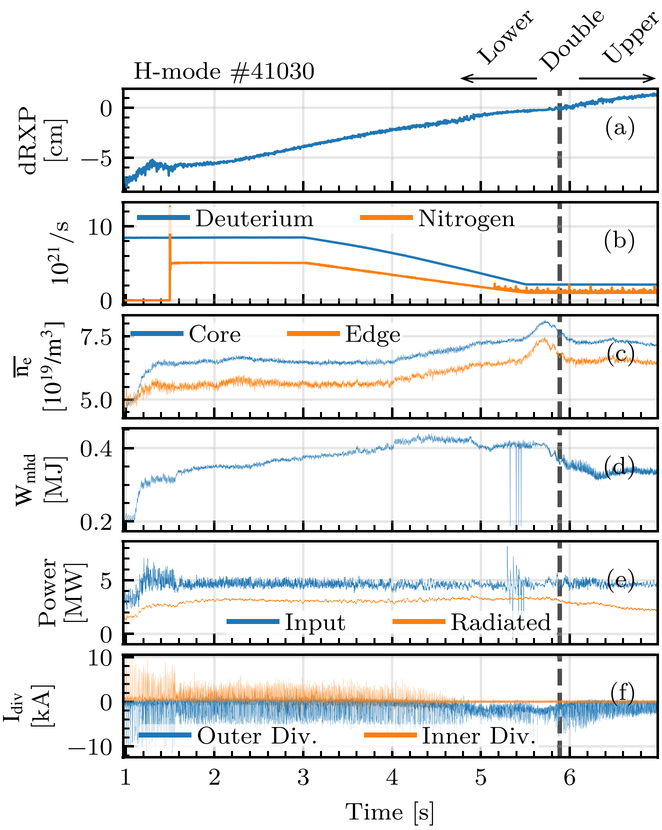

Figure 5. Main plasma parameters for the H-mode configuration scan #41030 with a magnetic field of −2.5 T, a plasma current of 0.8 MA, an ECRH heating power of 1.8 MW, an NBI heating power of 2.5 MW, and a q_{95} between 5.2 and 6.0. (a) separation between the main and secondary separatrix at the LFS midplane dRXP; (b) core and edge line-averaged density; (c) deuterium and nitrogen fueling rate; (d) stored energy; (e) total input and radiated power; (f) HFS and LFS divertor shunt currents. The black vertical dashed line indicates the double-null phase.

3. Results

During a shape scan, as the plasma gradually moves from a lower single-null to a double-null shape, the secondary separatrix approaches the primary separatrix and the connected SOL becomes narrower, see figure 3. The effect of this gradual magnetic disconnection between the HFS and LFS SOL is especially noticeable on the HFS SOL, where cross-field transport is expected to be comparatively small. We will show that, during a shape scan, the HFS SOL profile gradually narrows as we approach the double-null shape.

3.1. A secondary plasma boundary for the HFS SOL

Figure 6 shows the electron density as a function of time and radial position. In panels (a) and (b), the electron density is measured at the HFS midplane along the reflectometry LoS shown in figure 1. In panels (c) and (d), the electron density is measured in the divertor region along the divertor Thomson scattering LoS, also shown in figure 1. The data shown in figure 6 are from shots #40085 and #40260, an L-mode and an H-mode shape scan, respectively. The electron density, represented in a color scale, is overlaid with time traces identifying the position of the primary and the secondary separatrices as obtained from the plasma equilibrium reconstruction. Note that, as reflectometry is limited to $n_e < 3 \times 10^{19}\mathrm{m}^{-3}$, density measurements are often restricted to a narrow region of the SOL. We indicate the region not accessible to reflectometry with a gray shade.

Figure 6 illustrates a behavior typically observed in these shape scans. In the four panels shown, the secondary separatrix roughly divides the SOL into two regions, a high-density region inside, and a low-density region outside, with a steep gradient between them. The high-density region inside the secondary separatrix has a much larger density than the LFS SOL, as will be shown later. In figure 6, the region between the primary and secondary separatrices is the connected HFS SOL (illustrated in figure 3) as it is magnetically connected to the LFS SOL. The region outside the secondary separatrix is the disconnected HFS SOL.

The strong correlation between the secondary separatrix and the HFS SOL density profile suggests that the parallel transport of heat from the LFS SOL is critical to establishing the high-density region in both the HFS midplane and divertor. In other words, the high-density front only exists on the HFS SOL along flux surfaces connected to the LFS SOL.

Note that when the plasma shape gets close to a double-null, the line-averaged density increases (see figures 4(c) and 5(c)). This increase makes it challenging to analyze the SOL profile evolution close to double-null, as both the plasma shape and its line-averaged density change simultaneously.

Note also the effect of the ELMs, which modulate the HFS SOL density in figure 6 panel (b). This modulation is a known effect typically observed in H-mode, where the high-density front reappears after each ELM crash [16, 28]. The effect of the ELMs is not visible in the Thomson scattering signal due to the lower temporal resolution compared to reflectometry.

In this paper, we primarily examine L-mode shot #40085 and H-mode shot #41030, representing our most successful and typical shots. However, figure 6 features H-mode shot #40260, unique for the having both reflectometry and divertor Thomson scattering data, though it did not cross the double-null phase due to a disruption.

3.2. The density gradient of the HFS and LFS SOL

To better analyze the steep density gradient at the secondary separatrix location, we now look at figure 7, which shows five snapshots of the midplane density profile as a function of the normalized poloidal flux coordinate ρ-poloidal for both the HFS in panel (a) and the LFS in panel (b). The profiles shown correspond to chronologically ordered dRXP values of −20 mm, −10 mm, −5 mm, 0 mm, and +5 mm. The density profile was smoothed radially to aid the visualization and the resulting radial resolution is ≈ 0.002 in ρ-poloidal units.

Figure 7 shows that the HFS and LFS midplane density profiles are different, i.e. there is poloidal asymmetry, with a higher density at the HFS. While the LFS SOL experiences

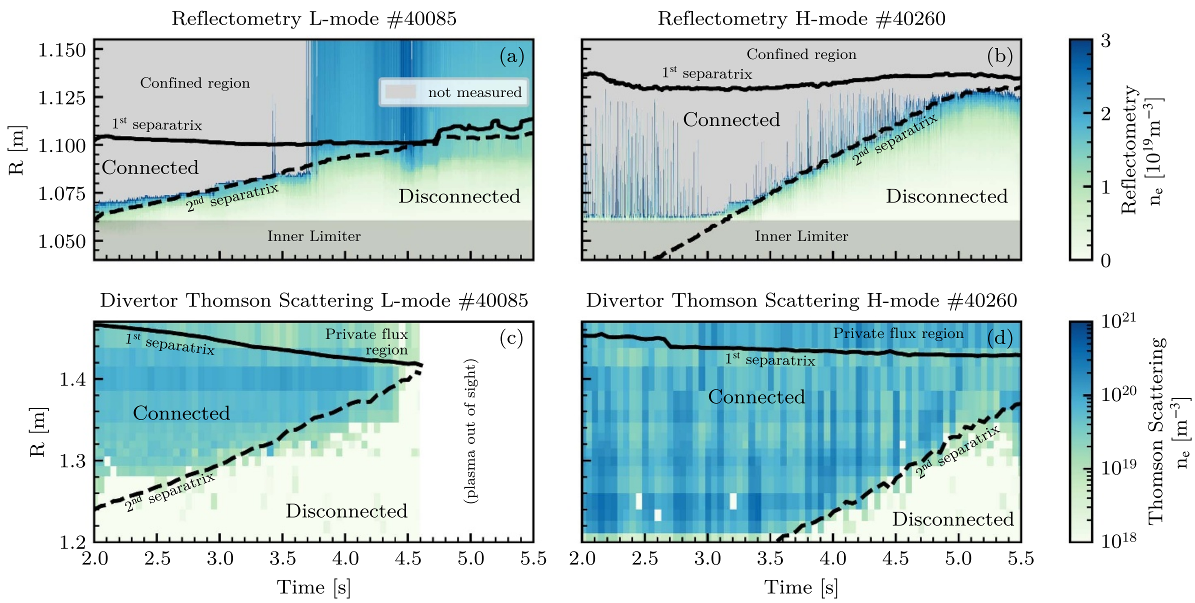

Figure 6. HFS SOL density contour as a function of time and major radius at the HFS midplane using O-mode reflectometry (panels (a) and (b)) and at the divertor using Thomson scattering (panels (c) and (d)) from an L-mode shape scan #40085 (panels (a) and (c)), and an H-mode shape scan #40260 (panels (b) and (d)). The black solid line gives the radial location of the primary separatrix and the black dashed line that of the secondary separatrix. The two lines divide the space into three regions, as illustrated in figure 3: the 'Disconnected' region below the secondary separatrix, the 'Connected' region between the secondary and the primary separatrix, and either the confined region (a) and (b) or the private flux region (c) and (d) above the primary separatrix. When the density near the secondary separatrix reaches 3×10^{19} m^{-3}, the reflectometer cannot probe beyond it and the unprobed region is indicated in a gray shade.

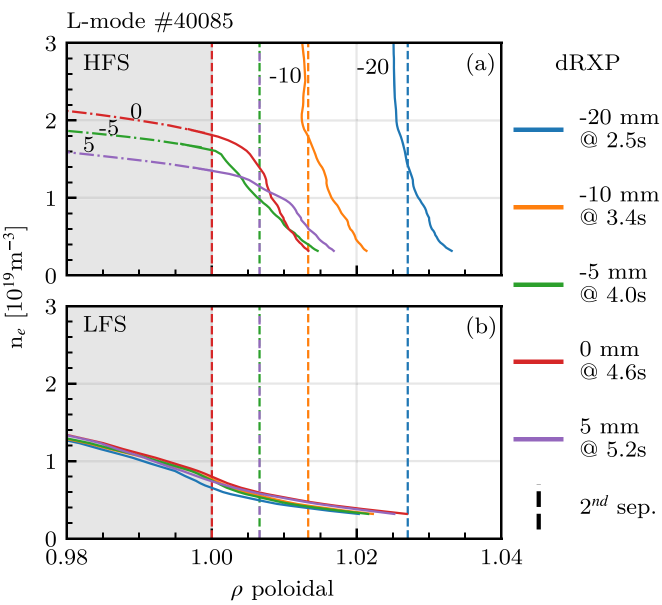

Figure 7. Midplane SOL density profile at the HFS (a) and LFS (b) for different dRXP values. Data from the L-mode shape scan #40085 measured using O-mode reflectometry. The vertical dashed lines indicate the position of the secondary separatrix for each different dRXP value. The HFS density profiles (panel a) for dRXP values -5, 0, and 5 may be overestimated in the confined region and are indicated with a dash-dot line style. The actual density profile for these three cases may be non-monotonic with a local maximum near the separatrix [17].

little change during the shape scan, the HFS SOL strongly depends on the plasma shape and the magnetic connection to the LFS SOL.

For dRXP values of -20 and -10 mm, the HFS midplane SOL density shoots up to values above 3×10^{19} m^{-3} combined with a steep gradient at the secondary separatrix location. In contrast, closer to the double-null shape, when dRXP is ±5 and 0, the peak density falls below 2×10^{19} m^{-3}, with a shallower density gradient, indicating a reduction of the density front magnitude.

There are also slight differences among the dRXP values of -5, 0, and $+5$ mm. The profiles in the upper single-null phase with a dRXP of 5 mm are broader than in the lower single-null phase with a dRXP of -5 mm. In the double-null phase, with a dRXP of zero, the density profile is affected by the increase in line-averaged density, making the comparison with other phases difficult.

Note that the high-density front on the HFS SOL might lead to a local density maximum meaning that the density will decrease radially as we move from the HFS SOL to the confined region. Under such circumstances, microwaves launched from the HFS are unable to accurately probe the region behind the high-density front. The end result is an overestimation of the density in the confined region [17]. For this reason, density profiles in the HFS confined region are represented with dashed lines in figure 7(a), as the real density might be significantly lower.

The LFS SOL density profiles shown in figure 7(b) were compared to other available diagnostics, showing a good agreement with all of them. Figure 7(b) shows that the LFS SOL profile does not change significantly, despite the changing magnetic configuration, except at dRXP = -20 mm, where the SOL density is slightly lower. Furthermore, the LFS SOL profile possesses no distinctive feature at the secondary

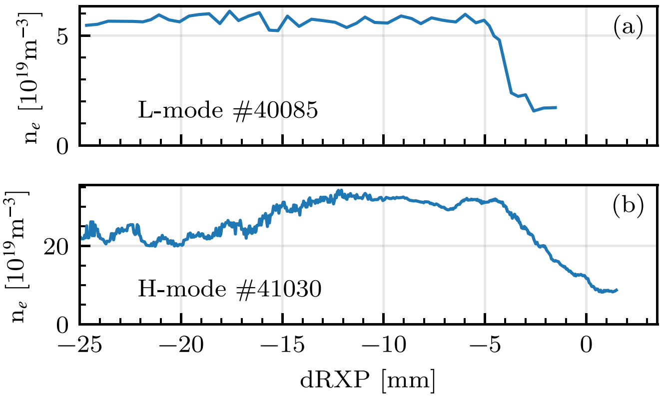

Figure 8. Average measurements of the HFS divertor Stark broadening spectroscopy system for the L-mode shape scan #40085 (a) and the H-mode shape scan #41030 (b). Average taken across all six lines of sight shown in figure 1. Data for the L-mode shot were only available until dRXP ≈ -1 mm. After that point, the spectrometer signal-to-noise ratio becomes too small. The same happens for the H-mode shot at a dRXP ≈ 2 mm.

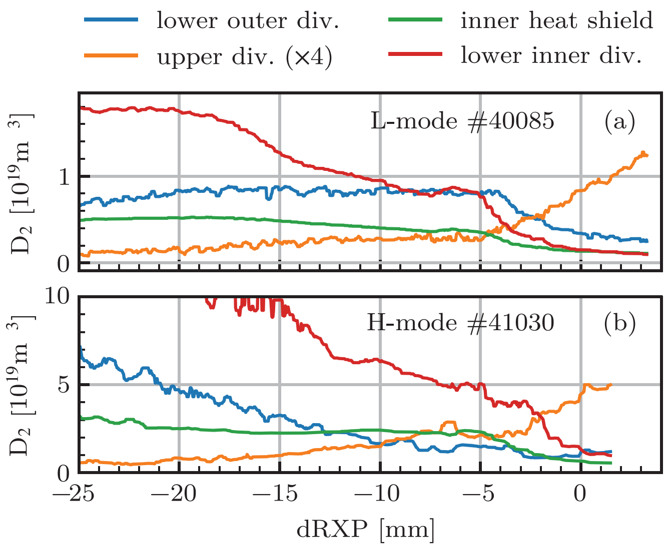

Figure 9. Neutral density measurements for the L-mode shape scan #40085 (a) and the H-mode shape scan #41030 (b). The neutral density is measured at different poloidal locations by the manometers shown in figure 1.

separatrix location, indicating that it does not depend on the magnetic connection to the HFS SOL.

3.3. The HFS divertor density near double-null

In addition to the divertor Thomson scattering system, ASDEX Upgrade possesses another diagnostic to measure the density in the divertor region.

Figure 8 shows density measurements from the Stark broadening divertor spectroscopy system as a function of dRXP for an L-mode and an H-mode shape scan. The data shown are a combination of the various LoS of the spectroscopy system shown in figure 1. The spectroscopy system roughly measures the maximum density along each LoS. Figure 8 shows the average across all LoS which serves here as an estimate for the high-density front magnitude in the HFS divertor.

As illustrated in figure 8(a), during the L-mode shape scan, when dRXP reaches -5 mm, the HFS divertor density experiences a steep decrease dropping from 6 to $2 \times 10^{19}\mathrm{m}^{-3}$. During the H-mode shape scan, figure 8(b), the density decrease is slower, starting at a dRXP of -4 mm, and going from 30 to $7 \times 10^{19}\mathrm{m}^{-3}$. These measurements indicate that the density front is reduced, albeit not completely, when approaching double-null.

3.4. Neutral density changes during the shape scan

We now focus on the neutral density measured by the manometers shown in figure 1. Figure 9 shows the neutral density at the lower and upper divertor and the HFS heatshield (just above the divertor) during an L-mode and an H-mode shape scans. As dRXP approaches zero, disconnecting the HFS and LFS SOL, the neutral density in the HFS divertor and heatshield decreases gradually. The decrease in neutral density is likely an indirect consequence of the reduced magnetic connection between the LFS SOL and HFS divertor. As the magnetic connection decreases, so does the magnitude of the high-density region, together with the associated ionization and neutral sources that sustain the high neutral pressures in the HFS divertor. When dRXP reaches -5 mm in L-mode, the lower divertor neutral density decreases steeply, and the upper divertor neutral density increases. The same happens in H-mode but at a slightly higher dRXP of -2.5 mm. This slight difference could be explained in terms of different power decay lengths between L-mode and H-mode as will be discussed later.

Recall from figures 7 and 8 that dRXP values greater than -5 mm lead to a substantial decrease in the high-density front. The same is true for the neutral density in the HFS divertor and heatshield shown in figure 9. There seems to be, therefore, a good correlation between the high-density front and the neutral density, which agrees with past modeling efforts [10].

3.5. The HFS divertor target

Having looked at the HFS midplane and divertor volume, we now turn to the HFS divertor target where the Langmuir probes indicated in figure 1 measure the electron temperature and density.

Figure 10 shows the Langmuir probe measurements along the lower HFS divertor target for the L-mode shape scan #40085. Two lines in the figure indicate the location of the primary and secondary strike points, where the primary and secondary separatrices intersect the divertor target. Similar to figure 6 where we showed the reflectometry and the Thomson scattering measurements, here, the secondary strike point also roughly divides the HFS target into two regions, one region with higher density between the primary and secondary strike

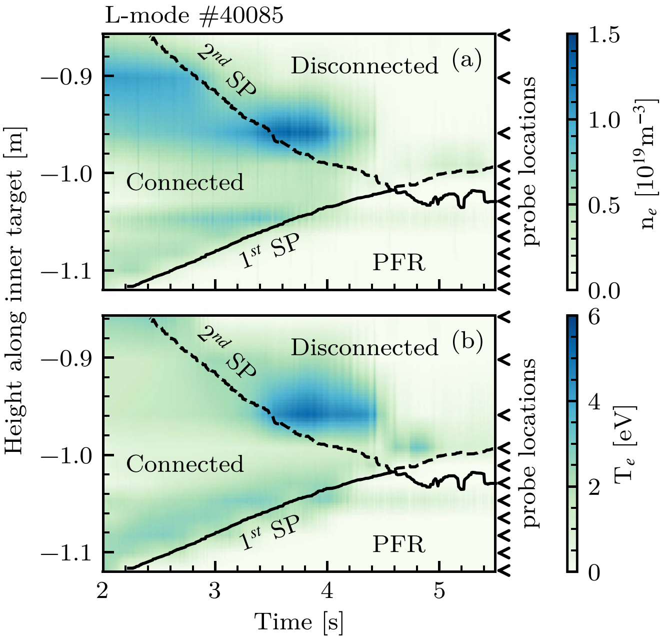

Figure 10. Langmuir probe measurements at the HFS target for the L-mode shape scan #40085. Electron density (a) and electron temperature (b). Data shown in a color scale as a function of time and height along the HFS target. Arrows on the right-hand side of each panel show the location of each Langmuir probe. The black solid line is the primary strike point (1st SP) and the black dashed line is the secondary strike point (2nd SP). The two lines divide the space into three regions, the private flux region (PFR) below the 1st SP, the 'Connected' region between the 1st SP and the 2nd SP, and the 'Disconnected' region above the 2nd SP.

points, and another region with lower density above the secondary strike point. However, at the divertor target, the separation between the two regions is not as steep as at the midplane or near the X-point, with one probe in particular registering an elevated density and temperature just outside the secondary strike-point location.

This observed behavior can potentially be attributed to the effect of E×B drifts redistributing particle flows in the divertor [10, 11], as this effect has been consistently observed across all shots studied. However, it is important to note that other mechanisms such as alternative neutral ionization pathways could also contribute to the observed spreading, and a comprehensive evaluation of these mechanisms was not performed in this study.

All experiments analyzed in this work, with the L-mode discharge shown in figure 10 being one example, are characterized by a partially or fully detached HFS divertor, identified as having an electron temperature below 5 eV [8]. Near double-null, the electron temperature and density at the strike point decrease, indicating a reduction of power conducted to the HFS target. During the shape scan, up to double-null, the region connected to the LFS always remains partially or fully detached.

Note that the probe coverage of the HFS target is poor, especially in the region where the secondary strike point sits. Nevertheless, it is evident that all diagnostics thus far agree that the secondary separatrix plays a critical role in establishing the HFS SOL profile.

4. Discussion and Conclusions

All the data presented so far show that the HFS SOL density profile strongly depends on the location of the secondary separatrix and on the critical parameter dRXP, i.e. the distance between the primary and secondary separatrix at the LFS midplane. This behavior differs from that of the LFS SOL, with almost no changes during the shape scans. The influence of the secondary separatrix was consistently observed in both L-mode and H-mode discharges. Experiments were conducted with varying seeding levels, including no seeding. These experiments yielded comparable outcomes concerning the impact of the secondary separatrix, although the peak density values in the HFS SOL varied.

We have observed steep density profiles coinciding with the secondary separatrix location at the HFS SOL. This observation supports a ballooning-like transport mechanism that favors losses at the LFS SOL. Without a magnetic connection between the HFS and LFS SOL, plasma losses at the LFS do not reach the HFS. Consequently, the high-density front only exists between the primary and secondary separatrices, and the HFS SOL profile narrows as the plasma approaches the double-null shape. Note that this is for a lower single-null shape with the B $\times$ ∇B direction pointing downwards.

Our findings at ASDEX Upgrade align with previous results from Alcator C-Mod where studies of SOL flows have found that 'plasma is preferentially lost near the equatorial midplane on the LFS and transits at high velocity along magnetic field lines to *fill in* the SOL on the HFS—a region that would otherwise be empty of plasma' [4].

In this paper we show that magnetically isolating the HFS SOL from the LFS SOL reduces the high-density region likely by reducing the heat flux to the HFS SOL. Our experiments show that progressively disconnecting the HFS SOL from the LFS leads to reduced electron and neutral densities in the HFS SOL and divertor. The density reduction is especially pronounced around specific dRXP values.

The phenomena discussed in this paper can be understood through the following explanation: The primary heat source in the SOL of a tokamak, as observed in various studies, is predominantly located around the LFS midplane, owing to a locally enhanced radial transport associated with the unfavorable curvature of the magnetic field [6, 29]. In the SOL, the heat is conducted along the magnetic field lines, reaching both the LFS divertor and the HFS SOL. On the HFS, radial transport is considerably weaker and the heat reaching the HFS SOL originates primarily from the LFS SOL through parallel heat conduction and near-sonic flows, as noted in multiple tokamaks [2, 30, 31].

Crucially, this parallel heat transport is restricted to field lines that connect the HFS and LFS SOL. Therefore, the secondary separatrix acts as a boundary, beyond which parallel transport is no longer a relevant heat source in the HFS SOL. Moreover, the density decreases sharply outside the secondary separatrix. This corroborates the fact that the large density in the HFS SOL is sustained by the parallel heat transport from the LFS. It has been shown, both experimentally and in simulations, that the magnitude of the high-density region in the HFS divertor increases with the power into the region of strong ionization [10, 12]. The high-density region forms under conditions of high gas fueling and heating power. Conversely, impurity seeding reduces the density, as it diminishes the heat flux to the HFS divertor. The lower heat flux fails to maintain the high-density region due to insufficient ionization [10, 12]. The power that reaches the HFS divertor is essential to maintain the high-density region and this dependence has been well established in literature [10, 12]. Consequently, it is expected that without the heat flux from the LFS, the HFS SOL cannot maintain a large density outside the secondary separatrix, leading to a steep density gradient across the HFS SOL.

At some point during the transition from a lower single-null shape to a double-null, a significant portion of the heat flow is redirected toward the upper divertor, no longer reaching the HFS SOL. We expect this to occur when the dRXP value approaches the power decay length. To estimate the power decay length λ_{q_e}, we use the electron temperature decay length λ_{T_e} and the formula $\lambda_{q_e} = 2\lambda_{T_e}/7$, which assumes a conduction-limited regime [32]. The electron temperature decay length is obtained from the edge Thomson scattering diagnostic, see figure 1.

For the L-mode plasmas studied here, we measured a λ_{T_e} of ≈ 13 mm, yielding a power decay length λ_{q_e} of ≈ 4 mm. The power decay length in H-mode was naturally shorter than in L-mode, with $\lambda_{T_e} \approx 9$ mm, giving us $\lambda_{q_e} \approx 3$ mm. The observations made here suggest that the HFS divertor electron density decreases rapidly after a certain dRXP value. In L-mode, we have observed a density decrease at a dRXP of approximately -5 mm while in H-mode we have observed a density decrease at a dRXP closer to zero (-5 to -2.5 mm). These observations are broadly consistent with the estimated λ_{q_e}, confirming that the high-density front magnitude decreases when the width of the magnetically connected region falls below λ_{q_e} at the LFS midplane.

Unlike the midplane HFS SOL, the midplane LFS SOL experiences almost no changes going from a lower single-null shape to a double-null. This is to be expected as the LFS radial transport is mostly a consequence of the local enhanced losses resulting from the bad curvature. Furthermore, our data show that there seems to be a one-way causal link between the LFS SOL and the HFS SOL where magnetically disconnecting the two sides affects only the HFS. This indicates that the LFS SOL profile is dictated by local transport phenomena while the HFS SOL profile is dictated by parallel transport from the LFS.

Closer to double-null, when the magnetic connection is negligible, the density profile is less influenced by the exact location of the secondary separatrix. In our experiments, we observe a minimum HFS SOL width obtained near the double-null phase, i.e. there seems to be a lower bound on the HFS SOL width. However, this minimum width is difficult to interpret due to excursions of the line-averaged density, and differences between the lower and upper divertor, particularly with respect to pumping. For both L-mode and H-mode discharges the minimum HFS SOL width was ≈ 10 mm, or ≈ 5 mm when mapped to the LFS midplane. This width was obtained by measuring the radial distance between the separatrix and a density layer approximately in the region of steepest gradient in the HFS SOL. For the L-mode shot, the SOL width was measured at $1 \times 10^{19}\,\mathrm{m}^{-3}$. For the H-mode shot, the SOL width was measured at $3 \times 10^{19}\,\mathrm{m}^{-3}$. This ensured that the selected density layer corresponded to a density smaller than the high-density front. Although arbitrarily defined, this width measurement gives a rough figure of merit for the behavior of the HFS SOL near double-null. Note that the density e-folding length, often used to characterize the SOL width, is unsuitable to characterize the HFS SOL width due to the steep density gradient often observed at the secondary separatrix location.

Comparing the midplane density profiles at the LFS and HFS SOL, we observed evident asymmetries with a larger density at the HFS SOL due to the existence of the high-density front. The HFS/LFS asymmetry lessens near double-null. The HFS density is nonetheless larger than the LFS even in double null both in the midplane and divertor.

Compared to the lower, the upper single-null shape shows a smaller HFS SOL density as can be observed in figure 7(a). We speculate that this difference can be explained in terms of the E×B drift reversal, as suggested by modeling [8, 10]. In a lower single-null shape with a downwards $B \times \nabla B$ direction, the E×B drift points from the LFS divertor to the HFS divertor pushing particles to the HFS divertor and fueling the high-density front. In an upper single-null shape with the same toroidal magnetic field, the E×B drift points from the HFS divertor to the LFS divertor therefore reducing the high-density front in the HFS SOL. However, the lower and upper divertors at ASDEX Upgrade are very different in terms of geometry and pumping, hampering a fair comparison between lower and upper single-null. To better observe the effect of the reversed E×B drift, we would need to compare shots in lower-single null but with different magnetic field directions. This is, however, outside the scope of this work which focuses primarily on the changes in the HFS SOL going from a lower single-null to double-null shape.

During the shape scans analyzed here, both in L-mode and H-mode, the HFS divertor remained partially or fully detached throughout, with low temperatures in L-mode (<5 eV) and slightly higher temperatures in H-mode near the strike point (5–10 eV). In H-mode, we observed reattachment of the HFS divertor following each ELM crash. Close to double-null, the reduction in heat flow from the LFS SOL to the HFS target led to a reduction in temperature and density.

In conclusion, these experiments, conducted at ASDEX Upgrade, demonstrate a strong correlation between the secondary separatrix location and the HFS SOL profile, highlighting the importance of the magnetic connection between the HFS and LFS SOL and the parallel heat conduction, as well as the ballooning nature of radial transport. The data shown here can be compared to computer simulations like the SOLPS code and others to further refine modeling accuracy in highly shaped plasmas.

Modeling will also allow a more quantitative physics understanding of these experimental results. Lastly, we observed that the HFS divertor remained detached during the shape scan with no significant increase in heat-flux to the target.

Data availability statement

All data that support the findings of this study are included within the article (and any supplementary files).

Acknowledgments

This work has been carried out within the framework of the EUROfusion Consortium, funded by the European Union via the Euratom Research and Training Programme (Grant Agreement No 101052200—EUROfusion). Views and opinions expressed are however those of the author(s) only and do not necessarily reflect those of the European Union or the European Commission. Neither the European Union nor the European Commission can be held responsible for them. IPFN activities received financial support from 'Fundação para a Ciência e Tecnologia' through Projects UIDB/50010/2020, UIDP/50010/2020, and PD/00505/2012 in the framework of the Advanced Program in Plasma Science and Engineering (APPLAuSE).

ORCID iDs

D Hachmeister https://orcid.org/0000-0002-1420-4376
C Silva https://orcid.org/0000-0001-6348-0505
J Santos https://orcid.org/0000-0002-9329-2457
G D Conway https://orcid.org/0000-0002-3947-4268
L Gil https://orcid.org/0000-0002-9970-2154
A Silva https://orcid.org/0000-0002-0003-7263
U Stroth https://orcid.org/0000-0003-1104-2233
E Wolfrum https://orcid.org/0000-0002-6645-6882
R M McDermott https://orcid.org/0000-0002-8958-8714
R Dux https://orcid.org/0000-0002-3447-9553
D Brida https://orcid.org/0000-0002-8647-7058

References

[1] Smick N, Labombard B and Pitcher C S 2005 Plasma profiles and flows in the high-field side scrape-off layer in Alcator C-Mod *J. Nucl. Mater.* **337–339** 281–285
[2] Boedo J A 2009 *J. Nucl. Mater.* **390–391** 29–37
[3] Tamain P, Bufferand H and Ciraolo G 2014 *Contrib. Plasma Phys.* **54** 555–559
[4] Smick N, Labombard B and Hutchinson I 2013 *Nucl. Fusion* **53** 023001
[5] Labombard B, Kuang A Q and Brunner D 2017 *Nucl. Mater. Energy* **12** 139
[6] Gunn J P, Boucher C and Dionne M 2007 *J. Nucl. Mater.* **363–365** 484
[7] Silva C, Arnoux G and Devaux S 2014 *Nucl. Fusion* **54** 083022
[8] Potzel S, Wischmeier M and Bernert M 2014 *Nucl. Fusion* **54** 013001
[9] Leonard A W 2018 *Plasma Phys. Control. Fusion* **60** 044001
[10] Reimold F, Wischmeier M and Potzel S 2017 *Nucl. Mater. Energy* **12** 193
[11] Korving S Q, Huijsmans G T, Park J S and Loarte A 2023 *Phys. Plasmas* **30** 042509
[12] Potzel S, Wischmeier M and Bernert M 2015 *J. Nucl. Mater.* **463** 541
[13] Guimarais L, Potzel S and Silva C 2018 *Nucl. Fusion* **58** 026005
[14] Krasheninnikov S I, Pigarov A Y and Knoll D A 1997 *Phys. Plasmas* **4** 1638
[15] Lipschultz B, Terry J L and Boswell C 1999 *J. Nucl. Mater.* **266-269** 370
[16] Guimarais L, Silva C and Bernert M 2019 *Nucl. Fusion* **59** 126041
[17] Hachmeister D, Silva C and SANTOS J 2022 *J. Instrum.* **17** C01008
[18] Iter O 2018 ITER research plan within the staged approach (Level III-Provisional Version) *Technical Report* ITR-18-003
[19] Kamada Y, Barabaschi P and Ishida S 2011 *Nucl. Fusion* **51** 073011
[20] Creely A J, Greenwald M J and Ballinger S B 2020 *J. Plasma Phys.* **86** 865860502
[21] Silva A, Manso M E and Cupido L 1996 *Rev. Sci. Instrum.* **67** 4138
[22] Varela P, Manso M E, Silva A, Fernandes J and Silva F 1995 *Rev. Sci. Instrum.* **66** 4937
[23] Kurzan B and Murmann H D 2011 *Rev. Sci. Instrum.* **82** 103501
[24] Brida D, Silvagni D, Eich T, Faitsch M and Mccarthy P 2020 *Plasma Phys. Control. Fusion* **62** 105014
[25] Kurzan B, Lohs A, Sellmair G, Sochor M and Team A U 2021 *J. Instrum.* **16** C09012
[26] Haas G and Bosch H S 1998 *Vacuum* **51** 39–46
[27] Fischer R *et al* 2017 *Fusion Sci. Technol.* **69** 526–36
[28] Laggner F M, Keerl S and Gnilsen J 2017 *Plasma Phys. Control. Fusion* **60** 025002
[29] Fedorczak N, Gunn J and Ghendrih P 2011 *J. Nucl. Mater.* **415** S467–70
[30] Labombard B, Rice J E and Hubbard A E 2004 *Nucl. Fusion* **44** 1047
[31] Pitts R, Andrew P and Bonnin X 2005 *J. Nucl. Mater.* **337–339** 146
[32] Sun H J, Wolfrum E and Kurzan B (ASDEX Upgrade Team) 2017 *Plasma Phys. Control. Fusion* **59** 105010